*Original Article*

JCBFM

Journal of Cerebral Blood Flow & Metabolism
2024, Vol. 44(3) 367–383
© The Author(s) 2023
Article reuse guidelines:
sagepub.com/journals-permissions
DOI: 10.1177/0271678X231214838
journals.sagepub.com/home/jcbfm
Sage

# CCL5 mediated astrocyte-T cell interaction disrupts blood-brain barrier in mice after hemorrhagic stroke

**Shiyi Zhou[1,*], Chang Liu[1,*], Jixian Wang[2,*], Jing Ye[1,*], Qianyuan Lian[1], Lin Gan[1], Shiyu Deng[1], Tongtong Xu[1], Yiyan Guo[1], Wanlu Li[1], Zhijun Zhang[1], Guo-Yuan Yang[1] and Yaohui Tang[1]**

## Abstract

The crosstalk between reactive astrocytes and infiltrated immune cells plays a critical role in maintaining blood-brain barrier (BBB) integrity. However, how astrocytes interact with immune cells and the effect of their interaction on BBB integrity after hemorrhagic stroke are still unclear. By performing RNA sequencing in astrocytes that were activated by interleukin-1α (IL-1α), tumor necrosis factor α (TNFα), and complement component 1q (C1q) treatment, we found CCL5 was among the top upregulated genes. Immunostaining and western blot results demonstrated that CCL5 was increased in mice brain after hemorrhagic stroke. Flow cytometry showed that knockout of astrocytic CCL5 reduced the infiltration of $CD8^+$ but not $CD4^+$ T and myeloid cells into the brain ($p < 0.05$). In addition, knockout CCL5 in astrocytes increased tight junction-related proteins ZO-1 and Occludin expression; reduced Evans blue leakage, perforin and granzyme B expression; improved neurobehavioral outcomes in hemorrhagic stroke mice ($p < 0.05$), while transplantation of $CD8^+$ T cells reversed these protective effects. Moreover, co-culture of $CD8^+$ T cells with bEnd.3 cells induced the apoptosis of bEnd.3 cells, which was rescued by inhibiting perforin. In conclusion, our study suggests that CCL5 mediated crosstalk between astrocytes and $CD8^+$ T cells represents an important therapeutic target for protecting BBB in stroke.

## Keywords

Astrocytes, blood-brain barrier, CCL5, intracerebral hemorrhage, T cells

Received 8 June 2023; Revised 17 October 2023; Accepted 24 October 2023

## Introduction

Blood-brain barrier (BBB) is a biological and functional barrier in the central nervous system (CNS) and serves as a dynamic metabolic interface.[1] Under normal physiological conditions, the BBB restricts the access of peripheral immune cells and molecules to the CNS for maintaining brain homeostasis.[2] As a key component of BBB, astrocytes play important roles in regulating and maintaining the barrier properties of the endothelial cells (ECs).[3] After hemorrhagic stroke, astrocytes transform into "reactive astrocytes", accumulate in the peri-hematoma area and participate in regulating the function of the BBB.[4–6] Studies showed that abundant reactive astrocytes were observed in the hyperacute and acute phases of hemorrhagic stroke, and inhibition of astrocyte activity reduced the size of hematoma enlargement and BBB disruption.[7] Recently, numerous studies demonstrated that reactive astrocytes contributed to BBB disruption and neurological deficits via interacting with immune cells.[8,9] However, how reactive astrocytes interact with

[1]Shanghai Sixth People's Hospital and School of Biomedical Engineering, Shanghai Jiao Tong University, Shanghai, China
[2]Department of Rehabilitation Medicine, Ruijin Hospital, School of Medicine, Shanghai Jiao Tong University, Shanghai, China

*These authors contributed equally to this work.

**Corresponding author:**
Yaohui Tang, Med-X Research Institute and School of Biomedical Engineering, Shanghai Jiao Tong University, Shanghai 200030, China.
Email: yaohuitang@sjtu.edu.cn

immune cells and the effects of astrocyte-immune cell interaction on BBB integrity after hemorrhagic stroke are still unclear.

During hemorrhagic stroke, peripheral immune cells including macrophages and T cells, could migrate to the injured site through the damaged BBB and activate inflammatory response, leading to secondary injuries in the peri-hematoma area, such as edema, inflammation, BBB disruption, cell necrosis and apoptosis.[10–13] It has been well-documented that astrocyte-derived chemokines are important drivers for inducing the migration of immune cells during immune surveillance and inflammatory responses.[14] In multiple sclerosis (MS), activated astrocytes recruited T lymphocytes to the CNS via CCL20, CXCL10, CXCL12, and CCL2, which caused BBB breakdown by inducing tight junction protein dismantlement.[15] In the experimental autoimmune encephalomyelitis (EAE) model, astrocyte-derived CCL2 recruited macrophages and T lymphocytes to the brain parenchyma and induced axon and myelin loss.[16] Our previous RNA sequencing study showed that many chemokines including CCL5, CCL7, CXCL5 etc. were highly up-regulated in reactive astrocytes,[17] leading us to hypothesize that these chemokines could mediate the interaction between astrocytes and immune cells, and further affect the neurological function.

Herein, by specifically knockout of CCL5 in astrocytes, we demonstrated that astrocyte-derived CCL5 mediated $CD8^+$ T cells infiltration into hemorrhagic stroke mice, and $CD8^+$ T cells induced endothelial apoptosis by perforin/granzyme B. Our study uncovered a novel mechanism of crosstalk between astrocytes and $CD8^+$ T cells, and elucidated how this crosstalk disrupted BBB in hemorrhagic stroke mice.

## Material and methods

### Animal experiments

Experimental animal studies were performed in accordance with the Animal Research: Reporting *in Vivo* Experiments (ARRIVE) guidelines. All animal experiments were conducted in accordance with Bioethics/2012022, Shanghai Jiao Tong University, Shanghai, China. Protocols were approved by Institutional Animal Care and Use Committee (IACUC) of Shanghai Jiao Tong University. This study used age- and sex-matched mice. Adult C57BL/6J mice (22–25 g, 8–10 weeks) were purchased from Vital River Laboratories (Vital River Laboratories, Beijing, China). Self-bred astrocytes specific knockout CCL5 mice ($Aldh1l1^{CreERT2+/-}$: $CCL5^{f/f}$ mice, 22–25 g, 10–12 weeks) were used. The transgenic mice were live, fertile, and normal-sized, without showing serious physical or behavioral abnormalities. Mice were housed in standard facilities with 12 h light-dark cycles with free access to food and water. The ambient humidity was controlled within 20∼50%, and the temperature was maintained at 21∼25°C. The wild-type mice used in the study were male, while the transgenic mice were both male and female, as detailed in figure legends. A total of 65 wild-type mice were used, and 11 mice were excluded due to death or surgery failure. A total of 200 transgenic mice were used. After excluding dead mice and failed models, 167 transgenic mice were used, including 92 male mice and 75 female mice. The number of mice in each group for neurobehavioral testing was 9–14, and the number of mice in each group was 3–8 in other experiments (specified in figure legends). Mice were randomly divided into groups for the experiments. Statistical data were obtained and analyzed in a double-blind manner.

### Generation of $Aldh1l1^{CreERT2+/-}$: $CCL5^{f/f}$ mice

To generate $Aldh1l1^{CreERT2+/-}$: $CCL5^{f/f}$ mice, loxp floxed CCL5 mice (purchased from GemPharmatech Co., Ltd, Jiangsu, China) were mated with $Aldh1l1^{CreERT2+/-}$ mice (a gift from Dr. Won-Suk Chung, Korea Advanced Institute of Science & Technology), and PCR was used to identify the genotype of the mice. Mice were used for experiments when they reach 10–12 weeks of age. Tamoxifen (Sigma-Aldrich, MO, USA) was dissolved in 95% corn oil at a final concentration of 10 mg/mL. Intraperitoneal injections of tamoxifen or corn oil into the experimental group or control group were started 2 weeks before experiments, once a day (0.075 mg/g body weight) for 5 consecutive days.

### Collagenase-induced intracerebral hemorrhage model

The intracerebral hemorrhage (ICH) mouse model was induced following the procedure as previously described.[18–20] Mice were anesthetized with 3% isoflurane mixed with 30% $O_2$/70% $N_2$, and 1.5% isoflurane mixed with 30% $O_2$/70% $N_2$ to maintain anesthesia by isoflurane gasifier (RWD Life Science Co., Shenzhen, China). The mouse head was then fixed on a stereotaxic instrument (RWD Life Science Co.) and ICH was performed using collagenase IV (Sigma-Aldrich). A small hole was drilled with a 29-gauge needle at 2 mm lateral to the midline and 0.5 mm anterior to the posterior fontanel. Then a 29-gauge needle containing collagenase IV was pushed to 3.5 mm of the right striatum. Each mouse was injected with 0.04 U collagenase IV dissolved in 2 μL 1X PBS using a micro-infusion pump (RWD Life Science Co.) at a speed of

0.4 μL/min. After surgery, animals were allowed to regain consciousness on a 37 °C heating pad (RWD Life Science Co.).

### Tissue collection

Under anesthesia, the mice were perfused with 1X PBS. And then the brain was quickly removed and placed on a cold dissection mold. The brain was cut into a 2 mm-thick slice before and behind the center of the injection site.

For western blot, the ipsilateral striatum isolated from the brain slice was transferred into cold protein lysis buffer (RIPA, PMSF, protease cocktail inhibitor and phosphatase inhibitor). Two small magnetic beads were placed into each sample tube and ground in a tissue grinder with shaking at 60 Hz for 45 sec. Lysates were centrifuged at 12,000 *g* for 20 min to obtain the supernatant.

For real time PCR, the ipsilateral striatum isolated from the brain slice was transferred into cold TRIzol reagent (Invitrogen, Waltham, MA). Two small magnetic beads were placed into each sample tube and ground in a tissue grinder with shaking at 60 Hz for 45 sec. Lysates were centrifuged at 12,000 *g* for 20 min to obtain the supernatant. The cell samples could be directly centrifuged to obtain the supernatant without the addition of small magnetic beads for grinding.

To collect brain slices, mice were perfused with 1X PBS and 4% paraformaldehyde (PFA, Sinopharm Chemical Reagent Co. Shanghai, China) under anesthesia, followed by immediate removal of the mouse brain. Brain sample was fixed in 4% PFA for 2 h, fully dehydrated in 30% sucrose solution until it sank, and then snap-frozen at −80°C in isopentane. Brains were embedded in optimal cutting temperature (OCT) compound (Fisher HealthCare, Waltham, MA) for frozen sectioning. Brain tissue slices were collected from anterior commissure to hippocampus.

### Western blot

Protein concentration of brain was determined by bicinchoninic acid (BCA) kit (Meilunbio, Dalian, China). The protein was denatured with instant protein loading buffer (EpiZyme, Shanghai, China) followed by boiling for 5 min. Equal amounts of protein from different samples were loaded on a 7.5%–12.5% (W/V) sodium dodecyl sulfate-polyacrylamide gel electrophoresis (SDS-PAGE) for electrophoresis. It was then transferred to a polyvinylidene fluoride (PVDF) membrane (Millipore, Burlington, MA). After that, membranes were blocked with protein-free rapid blocking buffer (EpiZyme) for 15 min at room temperature (RT), followed by incubation with the primary antibodies overnight at 4 °C. The following primary antibodies were used: CCL5 (1:800, sc-373984, Santa Cruz, Dallas, TX), ZO-1 (1:1000, 61-7300, Invitrogen), Perforin 1 (1:1000, sc-136994, Santa Cruz), Granzyme B (1:1000, sc-8022, Santa Cruz), and β-actin (1:5000, 66009, Invitrogen). Next day, the membrane was incubated with horseradish peroxidase (HRP)-conjugated secondary antibodies for 1 h at RT. The blots were imaged by incubation with the solution in the Enhanced Chemiluminescence Kit (ECL, Pierce Waltham, MA). Results were analyzed using Image *J* software (NIH, Bethesda, MD, RRID: SCR_003070).

### Real-time PCR analysis

Brain samples were dissolved in TRIzol reagent and RNA was extracted with chloroform, and then precipitated with isopropanol. Finally, the RNA pellet was washed with 75% alcohol. RNA concentration was examined using a spectrophotometer (NanoDrop 1000, Thermo Fisher, Waltham, MA). Single-stranded cDNA was subsequently synthesized by the Universal cDNA Synthesis Kit (Qiagen Hilden, Germany) for 1 h at 42 °C, followed by 5 min at 95 °C. RNA expression was tested by a fast RT-PCR system (7900 HT, ABI, Foster City, CA) using Hieff qPCR SYBR Green Master Mix (Yeasen Biotech, Shanghai, China) under the following cyclic conditions: 95 °C for 5 min followed by 40 cycles of 95 °C for 10 s and 60 °C for 30 sec, then 95 °C for 15 sec, 60 °C for 15 sec and 95 °C for 15 sec. GAPDH was used as the control for tissues. Table 1 listed primer sequences for real-time PCR analysis. Quantification was performed using the comparative CT method ($2^{-\Delta\Delta CT}$), and all data were normalized to GAPDH expression.

### Immunofluorescence staining (IF) and RNAscope in situ hybridization

Brain sections or cells were fixed with 4% PFA for 10 min and washed in 1X PBS buffer for 5 min X 3 times, followed by treatment with 0.3% Triton X-100 (Sigma-Aldrich) for 10 min. Then they were blocked with 1% bovine serum albumin (BSA, Gbico, Waltham, MA) for 60 min at RT and then incubated with primary antibodies overnight at 4 °C. The following antibodies were used: mouse anti-CCL5 (1:200, sc-373984, Santa Cruz), rabbit anti-GFAP (1:200, AB5804, Millipore), rabbit anti-Iba-1 (1:200, 019-19741, WAKO, Osaka, Japan), rabbit anti-NeuN (1:200, abn78, Millipore), goat anti-CD31 (1:200, AF3628, R&D, Minneapolis, MN), rabbit anti-ZO-1 (1:200, 61-7300, Invitrogen), rabbit anti-Occludin (AF7644, Beyotime, Jiangsu, China), rat anti-CD4 (1:200, ab269348, Abcam, Cambridge, UK), and rabbit anti-CD8 (1:200, ab217344, Abcam). Next day, after rinsing with 1X PBS buffer for 10 min X 3 times,

**Table 1.** List of primer sequences.

| Genes | Forward primer | Reverse primer |
|---|---|---|
| *Ccl2* | GCTACAAGAGGATCACCAGCAG | GTCTGGACCCATTCCTTCTTGG |
| *Ccl5* | CCTGCTGCTTTGCCTACCTCTC | ACACACTTGGCGGTTCCTTCGA |
| *Ccl7* | CAGAAGGATCACCAGTAGTCGG | ATAGCCTCCTCGACCCACTTCT |
| *CCR1* | GCCAAAAGACTGCTGTAAGAGCC | GCTTTGAAGCCTCCTATGCTGC |
| *CCR3* | CCACTGTACTCCCTGGTGTTCA | GGACAGTGAAGAGAAAGAGCAGG |
| *CCR4* | GGACTAGGTCTGTGCAAGATCG | TGCCTTCAAGGAGAATACCGCG |
| *CCR5* | GTCTACTTTCTCTTCTGGACTCC | CCAAGAGTCTCTGTTGCCTGCA |
| *Ctgf* | TGCGAAGCTGACCTGGAGGAAA | CCGCAGAACTTAGCCCTGTATG |
| *Cxcl1* | TCCAGAGCTTGAAGGTGTTGCC | AACCAAGGGAGCTTCAGGGTCA |
| *Cxcl5* | CCGCTGGCATTTCTGTTGCTGT | CAGGGATCACCTCCAAATTAGCG |
| *Dner* | GGAGAGCTTTGCCAGTCCAAGA | TTCACAAGCGGAGCCGAAGTAC |
| *Fbln5* | CCTGTGTCAACACCTATGGCTC | CACACTCGTGTTGACAGAGGAAC |
| *Gapdh* | CATCACTGCCACCCAGAAGACTG | ATGCCAGTGAGCTTCCCGTTCAG |
| *Gbp6* | TCGAGAGTTCCATCTTGCAGGC | AGCAGCTCTTGCTCCTTCTCTG |
| *Glycam1* | AAGACTCAGCCCACAGATGCCA | CTCTGAAGATGGAAGGCTCCTTG |
| *Lect1* | TCCTTGAACTCTGTGGCGACCT | GGAGCACTGTTTCTCACGACTTC |
| *Mmp3* | CTCTGGAACCTGAGACATCACC | AGGAGTCCTGAGAGATTTGCGC |
| *Nnat* | GTGGTGGAGGAAGAGGGTTAAG | CACATTTTGGGGAGGGCTTTCG |
| *Npvf* | GCCTCATTTTCACAGCAAAGAAGG | CTTTTAGTTCTTGAAAACTGACACTT |
| *Ogn* | AACGACCTGGAATCTGTGCCTC | TCGCTCCCGAATGTAACGAGTG |
| *Ptx3* | AACAAGCTCTGTTGCCCATT | TCCCAAATGGAACATTGGAT |
| *Saa3* | GAGCCTGGGCTGCTAAAGTCAT | CACTCATTGGCAAACTGGTCAGC |
| *Sertm1* | CTGTTTCCCACATCGCTGTCCA | TCAGCCTCTGAAGAGCAATGATC |
| *Slc39a12* | CAATGTGCCAGCCTCCAACAGA | CCAATGAAGAGGAGAAGGCTGTG |
| *Tnfaip2* | TTCGCCTGCAAGATTCCAGTGC | GCTCCTGACTTCACTGCTTGGT |

brain sections or cells were incubated with the fluorescent conjugated secondary antibodies for 1 h at RT. Then they were washed again in 1X PBS buffer for 15 min X 3 times. The slides were mounted with anti-fluorescence quencher medium containing DAPI (Beyotime). Fluorescence images were collected at 40X or 63X magnification using inverted confocal laser-scanning systems (Leica, Wetzlar, Germany). Four fields were imaged in peri-lesion areas in each slice, and four slices with 200 μm intersegment were counted for each mouse brain.

RNAscope was performed according to the supplier's protocol (Advance Cell Diagnostics (ACD), Hayward, CA). In short, the slides were subjected to serially gradient dehydration at RT, and incubated with HybEz™ hybridization system (ACD). The slides were incubated with RNAscope hydrogen peroxide at RT for 10 min, and then incubated with RNAscope protease III at 40 °C for 30 min. Custom mouse CCL5 RNAscope probe, negative and positive control probes were designed and purchased from ACD.

## *Evans blue (EB) injection and immunoglobulin G (IgG) leakage measurement*

BBB permeability was assessed by measuring the extravasation of EB and IgG. Under anesthesia, EB solution (Sigma-Aldrich, 2% EB dye in saline, 4 mL/kg) was slowly injected into the left jugular vein of mice at 3 days of hemorrhagic stroke.[21] The mice were sacrificed via cardiac perfusion after 2 h of EB circulation. Both brain hemispheres were weighed, and then EB was extracted by homogenizing the tissue samples with 1 mL of 50% trichloroacetic acid solution, centrifuge at 21,000 *g* for 20 min and the supernatant was diluted with 100% ethanol at a ratio of 1:3. The amount of EB was quantified at 610 nm using a spectrophotometer (Bio-Tek, Winooski, VT).

IgG staining was performed to check for IgG leakage according to the supplier's protocol. In brief, the brain slides were blow-dried at RT for 10 min after removal from −80°C. This was followed by fixation with 4% PFA for 5 min, then treated with 0.3% Triton X-100 for another 10 min, and subsequent blocking with 0.3% hydrogen peroxide in methanol for 30 min. Nonspecific staining was first reduced by incubation with super blocking solution for 5 min, then incubated with HRP-labeled IgG antibody (Absin, Shanghai, China) for 10 min each. Immunoreactivity was then observed using DAB staining (Vector Labs, Burlingame, CA). Brain sections were counterstained with hematoxylin and rinsed with running water for 1 h. After dehydration by ethanol, brain sections were sealed with neutral resin. IgG images were collected

using bright-field microscopy (Leica). The mean integrated optical density (IOD) of IgG was quantified using the immunohistochemistry Image Analysis toolbox of Image *J* software (NIH). For each mouse, four sections with 200 μm intersegment were evaluated and imaged at 4 fields in each section in the perihemorrhagic region.

### Neurobehavioral tests

Neurobehavioral tests were performed according to a previously described procedure at 1, 3, 7, and 14 days after hemorrhagic stroke by an investigator blinded to experimental design and treatment.[22,23] The tests included modified neurological severity score (mNSS), elevated body swing test (EBST), rotarod test and grid walking test. mNSS consisted of a combination of motor, reflex, and balance tests. Severity scores ranged from 0 to 14, with 0 indicating normal and higher scores indicating more severe injury.[22]

EBST was used to assess asymmetric motor behavior. The mouse tail was lifted about 10 cm away from the platform, and the direction and frequency of the mouse head deviation from the vertical axis were recorded, 20 times in total. The results were calculated as the number of total turns divided by the number of turns to the left.

Rotarod test was used to assess balance, grip strength, and sensorimotor coordination. Mice were required to train for 3 consecutive days prior to surgery, with a slow increase in speed from 20 to 40 rpm/min in 5 min. After surgery, mice were tested at the indicated time points, 35 rpm/min for 5 min. 3 trials were performed for each mouse, and the time the mouse remained on the accelerated rotarod was recorded.

Grid walking test was used to assess impairments in descending motor control. The device consisted of a wire grid floor 32 cm/20 cm/50 cm (length/width/height) with 1 cm openings. Each mouse was placed individually in the center of the grid, allowed to freely explore the enclosure for 5 min, and behavior was recorded by a camera placed below. After viewing the images, the total number of limbs walking and the number of placement faults (foot faults) were counted. A fault was defined as a step where the paw was detached from the wire. The foot fault index was calculated as [(cont. faults-ipsi. faults)/total steps] $\times 100$.

### TdT-mediated dUTP nick end labeling (TUNEL) staining

The procedure of primary antibody staining in mouse brain or cells was consistent with the procedure of immunofluorescence staining. The following antibodies were used: goat anti-CD31 (1:200, AF3628, R&D), and rabbit anti-NeuN (1:200, abn78, Millipore). Next day, brain sections or cells were incubated for 1 h at RT with TUNEL reagent (Meilunbio) containing terminal deoxynucleotidyl transferase, fluorescent dUTP isothiocyanate, and fluorescent conjugated secondary antibodies. The slices were mounted with an anti-fluorescence quencher medium containing DAPI. Fluorescence images were collected at 40X magnification using inverted confocal laser-scanning systems (Leica). Four fields were imaged in peri-lesion areas in each slice, and four slices with 200 μm intersegment were counted for each mouse brain.

### Flow cytometry and RT-PCR of CCR1, CCR3, CCR4, and CCR5 in $CD4^+$ and $CD8^+$ T cells

Neural Tissue Dissociation Kit-Papain (Miltenyi Biotec; San Diego, CA) was used to obtain the single-cell suspensions according to the supplier's protocol. In brief, mice were perfused with cold 1X DPBS buffer (Meilunbio), and the ipsilateral brain was harvested and mechanically homogenized. After thoroughly mixing the minced material with the lyase mixture, the mixture was placed on the machine and incubated at 37 °C for 22 min. After debris removal and red blood cell lysis using Debris Removal Solution (Miltenyi Biotec) and Red Blood Cell Lysis Solution (Miltenyi Biotec), single-cell suspensions were incubated with flow antibodies at 4 °C for 30 min. The following antibodies were used: Percp-cy5.5 anti-mouse CD45 (103132, Biolegend, San Diego, CA), APC anti-mouse CD4 (100411, Biolegend), FITC-anti mouse CD8 (100705, Biolegend), APC anti-mouse/human CD11b (101211, Biolegend), Brilliant Violet 421 anti-mouse CD11c (117329, Biolegend), PE anti-mouse Ly-6C (127606, Biolegend), FITC anti-mouse Ly-6G (128007, Biolegend) and Fixable Viability Stain 510 (564406, Biolegend). Multicolor flow cytometry was performed on flow cytometer (FACS Aria SORP, BD, San Jose, CA). The data were analyzed by fluorescence-activated cell sorting using Flowjo software. Set up the gate according to the control sample. $CD4^+$ T cells, $CD8^+$ T cells and $CD45^+CD4^-/CD8^-$ cells were collected and the expressions of CCR1, CCR3, CCR4, and CCR5 on these cells were analyzed using Real time PCR.

### Extraction of $CD8^+$ T cells

EasySep Mouse $CD8^+$ T Cell Isolation Kit (StemCell, Vancouver, Canada) was used to extract $CD8^+$ T cells according to the supplier's protocol. In brief, spleens and lymph nodes were isolated from mice at 3 days after ICH. After transferring the cell suspension to

a flow tube (Corning Incorporated, Corning, NY), 50 μL/mL Isolation Cocktail was added and incubated for 10 min at RT. The RapidSpheres™ (125 μL/mL) were vortexed for 30 sec in advance and incubated at RT for 5 min. The recommended medium was added to achieve a volume of 2.5 mL and the cells were incubated in the magnet for 2.5 min to obtain $CD8^+$ T cells. Repeat this step 3 times. Finally, purified enriched $CD8^+$ T cells were transferred into new tubes, counted and used for subsequent experiments.

### Co-culture of bEnd.3 cells and T cells

bEnd.3 was obtained from Chinese Academy of Sciences stem cell bank. $CD8^+$ T cells were obtained from spleen and inguinal lymph nodes of mice at 3 days after ICH. bEnd.3 cells were cultured under Dulbecco's modified eagle medium (DMEM, HyClone, Logan, UT) supplemented with 10% (V/V) fetal bovine serum (FBS, Gibco, Carlsbad, NM) and 1% penicillin-streptomycin antibiotics (Gibco). When bEnd.3 cells and $CD8^+$ T cells were co-cultured in the RPMI 1640 medium (Gibco) containing 10% FBS, 1% penicillin-streptomycin antibiotics, 2 mM glutamine, and 0.004% mercaptoethanol. bEnd.3 cells were seeded in 10 cm dishes. When cells were 80% confluent, they were digested and seeded into coverslips in 24-well plates, and $CD8^+$ T cells were added to a transwell chamber (Millipore). To inhibit the activity of perforin/granzyme in $CD8^+$ T cells, 0.2 mM EGTA (Shanghai Yuanye Bio-Technology Co., Ltd., Shanghai, China) was used to treat $CD8^+$ T cells.

Viability of bEnd.3 cells was determined by CCK-8 assay (Meilunbio). After 24 h co-culture, $CD8^+$ T cells and chambers were removed, and the medium was discarded. After washing with 1X PBS buffer, the medium containing 10% CCK-8 was added. After 30 min of incubation in the incubator, the medium was transferred to 96-well plates. Absorbance was measured at 450 nm using a microplate reader. Cells could be stored at 4 °C for 2 weeks after fixation with 4% PFA and used for TUNEL staining.

### Statistical analysis

Sample sizes for animal studies were determined by a two-sided power analysis for the primary parameter with mean differences and standard deviations based on similar previously published results (power = 80%, a = 0.05).[24,25] All statistics were performed using Prism GraphPad 9 (GraphPad Software, San Diego, CA). Results were presented as mean±standard deviation (SD). The Kolmogorov-Smirnov normality test was initially performed on all datasets. For normally distributed continuous variables, comparisons between two groups were conducted by the two-tailed Student's test (equal variances) or Welch's t test (unequal variances), and comparing more than two groups with one independent variable was conducted by one-way analysis of variance (ANOVA) with Dunnett's multiple comparisons test (all groups compared with a control group, equal variances) or with Tukey's multiple comparisons test (comparisons between all groups, equal variances), or by Brown-Forsythe and Welch ANOVA tests with Dunnett T3 test (unequal variances). When comparing more than two groups with two independent variables, two-way ANOVA with Bonferroni multiple comparisons test was used. For continuous variables with non-normal distributions, the two-tailed Mann-Whitney test was used. In all analyses, $p < 0.05$ was considered statistically significant.

## Results

### CCL5 was markedly increased in reactive astrocytes

Our previous transcriptomic study showed that many chemokines including CCL5, CCL7, CXCL5 etc. were upregulated in IL-1α, TNFα and C1q induced reactive astrocytes.[17] RT-PCR analysis verified these up-regulated and down-regulated genes (Figure 1(a) and (b)), which is consistent with previous findings that human fetal astrocytes secrete large amounts of CCL5 protein upon activation with IL-1β [26] and that human astrocytoma cell lines, primary human and rat astrocytes all produce CCL5 upon incubation with TNFα/IL-1β.[27]

CCL5 is an important chemokine and plays a critical role in mediating immune cell migration.[27–29] Thus, we focused on investigating the role of CCL5 in mediating astrocyte-immune cell interaction. We first examined the expression of CCL5 at different time points after ICH. The results of RT-PCR and western blot showed that CCL5 was highly expressed in the brain at 1 and 3 days after hemorrhagic stroke (Figure 1(c) to (e)). To determine the cellular source of CCL5, immunofluorescence staining was performed. Co-staining of CCL5/GFAP, CCL5/NeuN, CCL5/Iba-1 and CCL5/CD31 revealed that CCL5 was expressed in astrocytes, neurons and microglia, but not in endothelial cells (Figure 1(f)). Subsequently, we utilized the RNAscope *in situ* hybridization combined with immunohistochemistry to further clarify the cellular localization of CCL5. Positive control and negative control were shown in Suppl. Fig. 1. The results showed CCL5 mRNA signal in $GFAP^+$ astrocytes, $IBA\text{-}1^+$ microglia, and Neun+ neurons, but not in endothelial cells (Figure 1 (g)), which is consistent with immunostaining results.

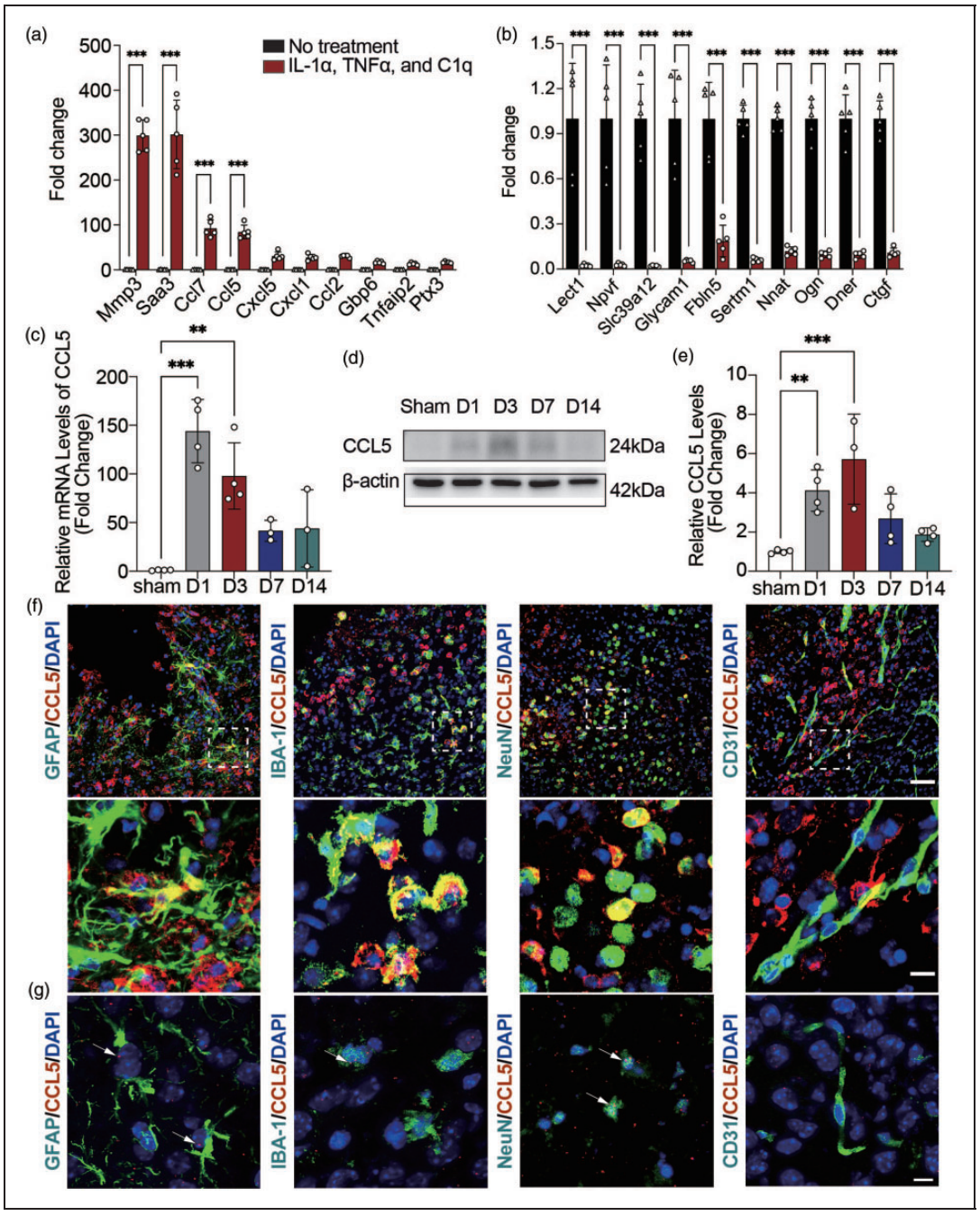


**Figure 1.** CCL5 levels increased markedly in reactive astrocytes. (a, b) RT-PCR analysis of 10 upregulated (a) and downregulated (b) genes between reactive astrocytes and resting astrocytes. n = 5 biologically independent primary astrocytes cultures. GAPDH was used as an internal control. Two-way ANOVA with Bonferroni multiple comparisons test. (c) RT-PCR analysis of CCL5 mRNA expression levels in the hemorrhagic perifocal area at 1, 3, 7, and 14 days after ICH. n = 4 mice in Sham/D1/D3 groups (all male), n = 3 mice in D7 and D14 groups (all male). GAPDH was used as an internal control. One-way ANOVA with Dunnett's multiple comparisons test. (d) Representative immunoblots of CCL5 protein expression levels in the hemorrhagic perifocal area at 1, 3, 7, and 14 days after ICH. (e) Quantification of CCL5 protein expression levels in the hemorrhagic perifocal area at 1, 3, 7, and 14 days after ICH. n = 4 mice in Sham/D1/D7/D14 groups (all male), n = 3 mice in D3 group (all male). β-actin was used as an internal control. One-way ANOVA with Dunnett's multiple comparisons test. (f) Representative immunostaining images of CCL5 (red) with astrocytes (GFAP, green), microglia (Iba-1, green), neurons (NeuN, green), and ECs (CD31, green) in the hemorrhagic perifocal area at day 3 of ICH. Above scale bar = 50 μm, below scale bar = 10 μm and (g) Representative RNAscope images of CCL5 mRNA (red) with astrocytes (GFAP, green), microglia (Iba-1, green), neurons (NeuN, green), and ECs (CD31, green) in the hemorrhagic perifocal area at day 3 of ICH. Scale bar = 10 μm. Arrows indicated the colocalization of astrocytes, microglia, and neurons with CCL5 mRNA, respectively. All data are presented as mean ± SD. $^{**}p < 0.01$, $^{***}p < 0.001$.

### *Knockout of CCL5 in astrocytes reduced CD8$^+$ T cells infiltration into hemorrhagic stroke brain*

To investigate if astrocytic CCL5 induces the infiltration of peripheral immune cells to the brain, CCL5 was specifically knockout in astrocytes (Aldh1l1$^{CreERT2+/-}$: CCL5$^{f/f}$) and hemorrhagic stroke was induced (Suppl. Fig. 2A). Both RT-PCR and western blot results showed that the expression of CCL5 was decreased in Aldh1l1$^{CreERT2+/-}$: CCL5$^{f/f}$ mice treated with tamoxifen, compared with oil-treated Aldh1l1$^{CreERT2+/-}$: CCL5$^{f/f}$ mice (Suppl. Figs. 2B, C, D).

We then analyzed the number of different immune cells in the hemorrhagic hemisphere of Aldh1l1$^{CreERT2+/-}$: CCL5$^{f/f}$ mice treated with tamoxifen (Tam ICH) or oil (Oil ICH), as well as Aldh1l1$^{CreERT2+/-}$: CCL5$^{f/f}$ sham mice treated with tamoxifen (Tam Sham) or oil (Oil Sham) by flow cytometry. Flow cytometry results showed the number of CD8$^+$ T cells (Figure 2(a)), CD4$^+$ T cells (Figure 2(b)), dendritic cells (Suppl. Fig. 3A), monocytes (Suppl. Fig. 3B) and neutrophils (Suppl. Fig. 3B) in Oil Sham mice, Tam Sham mice, Oil ICH mice and Tam ICH mice. CD4$^+$ T cells and CD8$^+$ T cells were gated according to the fluorescence intensity of CD45, and then according to CD3, CD4 and CD8 fluorescence intensity, respectively (Suppl. Fig. 4A). Dendritic cells, monocytes, and neutrophils were gated according to the fluorescence intensity of CD45 and CD11b staining, then according to the fluorescence intensity of CD11c, and finally according to the fluorescence intensity of Ly6C and Ly6G for further analysis (Suppl. Fig. 4B). As shown in Figure 2(c) and (d), minimal CD8$^+$ and CD4$^+$ T cells were found in both Oil Sham and Tam Sham mice. After hemorrhagic stroke, the number of CD8$^+$ T cells was reduced in Tam ICH mice compared with Oil ICH mice (Figure 2(c)), while the number of CD4$^+$ T cells was comparable between Tam ICH mice and Oil ICH mice (Figure 2(d)). Similarly, there were no significant changes in other immune cells after ICH (Suppl. Figs. 3C, D, E, F). We also used unbiased method tSNE to quantify infiltrating T cells and myeloid cells in hemorrhagic stroke brain. Our results showed that the number of CD8$^+$ T cells was reduced in Tam ICH mice (Suppl. Figs. 5A, B, C) compared with Oil ICH mice, while no difference in myeloid cells (Suppl. Figs. 5D, E, F).

We further verified the infiltration of CD8$^+$ T and CD4$^+$ T cells in the injured site of brain by immunofluorescence staining (Figure 2(e) and (f)). Statistical results of immunofluorescence staining showed that the number of CD8$^+$ T cells in the injury site was reduced in Tam ICH mice compared with Oil ICH mice (Figure 2(e)), while no significant change of the number of CD4$^+$ T cells between Tam ICH and Oil ICH group (Figure 2(f)), which was consistent with the flow cytometry results. We also detected the expression of CCL5 receptors including CCR1, CCR3, CCR4 and CCR5 on CD4$^+$ and CD8$^+$ T cells through RT-PCR. The results showed that the expression of CCL5 receptors CCR5 and CCR1, but not CCR3 and CCR4 in CD8$^+$ T cells was significantly higher than that in CD4$^+$ T cells (Suppl. Fig. 6). This may explain different effects of astrocytic CCL5 in mediating the migration of CD4$^+$ and CD8$^+$ T cells (Suppl. Fig. 6).

### *Knockout of CCL5 in astrocytes attenuated BBB disruption and neurobehavioral deficits*

To determine the role of astrocyte-derived CCL5 in regulating BBB integrity and neural function of mice after hemorrhagic stroke, we performed a variety of histological and neurobehavioral tests (Figure 3(a)). EB quantitative results showed that extravasation of EB was evident after ICH, whereas extravasation of EB was reduced in Tam ICH mice compared with Oil ICH mice (Figure 3(b)). We also examined IgG leakage to assess BBB integrity at day 3 after ICH. The location where IgG staining was taken is shown in the Suppl. Fig. 7. The results showed that IgG leakage was reduced in Tam ICH mice compared with Oil ICH mice (Figure 3(c)). Knockout of CCL5 in astrocytes reduced the loss of tight junction proteins ZO-1 and Occludin, as demonstrated by western blot analysis (Figure 3(d)) and immunofluorescence staining (Figure 3(e) and (f)). These results suggested that knockout of astrocytic CCL5 significantly alleviated BBB disruption in mice after hemorrhagic stroke.

To assess the effects of astrocytic CCL5 on the neurobehavior recovery of hemorrhagic stroke mice, we performed mNSS, EBST, rotarod test and grid walking test. We found that at 3, 7, and 14 days after ICH, Tam ICH mice had lower mNSS scores and better behavior in EBST compared with Oil ICH mice (Figure 4(a) and (b)). In addition, rotarod test showed that conditional knockout of CCL5 in astrocytes improved neurobehavioral recovery at 7 and 14 days after ICH compared with Oil ICH group (Figure 4(c)). Moreover, the Tam ICH group has better performance in grid walking test on 3$^{rd}$ day of ICH compared with the Oil ICH group (Figure 4(d)). Taken together, these results showed that CCL5 knockout in astrocytes alleviated BBB disruption and improved neurobehavioral outcomes in hemorrhagic stroke mice.

We also examined neuronal apoptosis at 3 days after ICH by TUNEL staining. The experimental results showed that the number of apoptotic neurons in the astrocyte-specific CCL5 knockout mice was reduced compared with the control mice (Suppl. Figs. 8A, B),

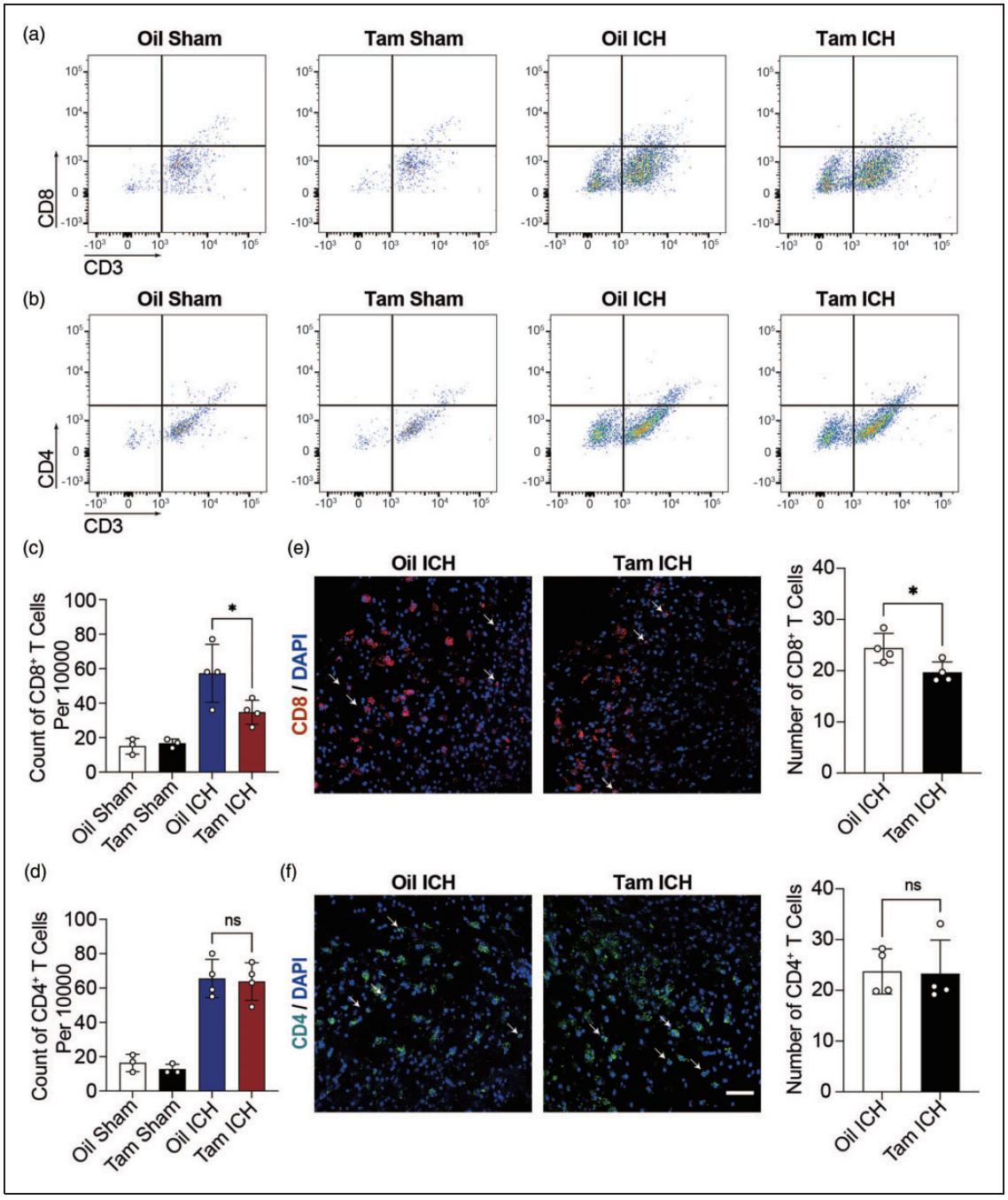


**Figure 2.** Knockout CCL5 in astrocytes reduced $CD8^+$ T infiltration. (a, b) Representative flow cytometry pseudocolor dot plots showed gating strategy of $CD8^+$ T cells ($CD3^+$ $CD8^+$) (a) and $CD4^+$ T cells ($CD3^+$ $CD4^+$) (b) in $Aldh1l1^{CreERT2+/-}$: $CCL5^{f/f}$ sham mice treated with oil (Oil Sham) or tamoxifen (Tam Sham), $Aldh1l1^{CreERT2+/-}$: $CCL5^{f/f}$ hemorrhagic stroke mice treated with oil (Oil ICH) or tamoxifen (Tam ICH). (c, d) The count of $CD8^+$ T cells ($CD3^+$ $CD8^+$) (c) and $CD4^+$ T cells ($CD3^+$ $CD4^+$) (d) per 10000 cells in Oil Sham, Tam Sham, Oil ICH and Tam ICH groups. n = 3 mice in Oil Sham group and Tam Sham group (1 female, 2 male), n = 4 mice in Oil ICH group (1 female, 3 male), n = 4 mice in Tam ICH group (2 female, 2 male). One-way ANOVA with Tukey's multiple comparisons test. (e) Representative immunostaining images of $CD8^+$ T cells (red) in the hemorrhagic perifocal area at day 3 of ICH. Arrowheads indicate $CD8^+$ T cells. The number of $CD8^+$ T cells in Oil ICH and Tam ICH groups in the hemorrhagic perifocal area at day 3 of ICH. n = 4 mice per group (all male). Two-sided, unpaired Student's test and (f) Representative immunostaining images of $CD4^+$ T cells (green) in the hemorrhagic perifocal area at day 3 of ICH. Scale bar = 50 μm. Arrowheads indicate $CD4^+$ T cells. The number of $CD4^+$ T cells in Oil ICH and Tam ICH groups in the hemorrhagic perifocal area at day 3 of ICH. n = 4 mice per group (all male). Two-sided, Mann-Whitney test. All data are presented as mean ± SD. *$p < 0.05$, ns, no significance.

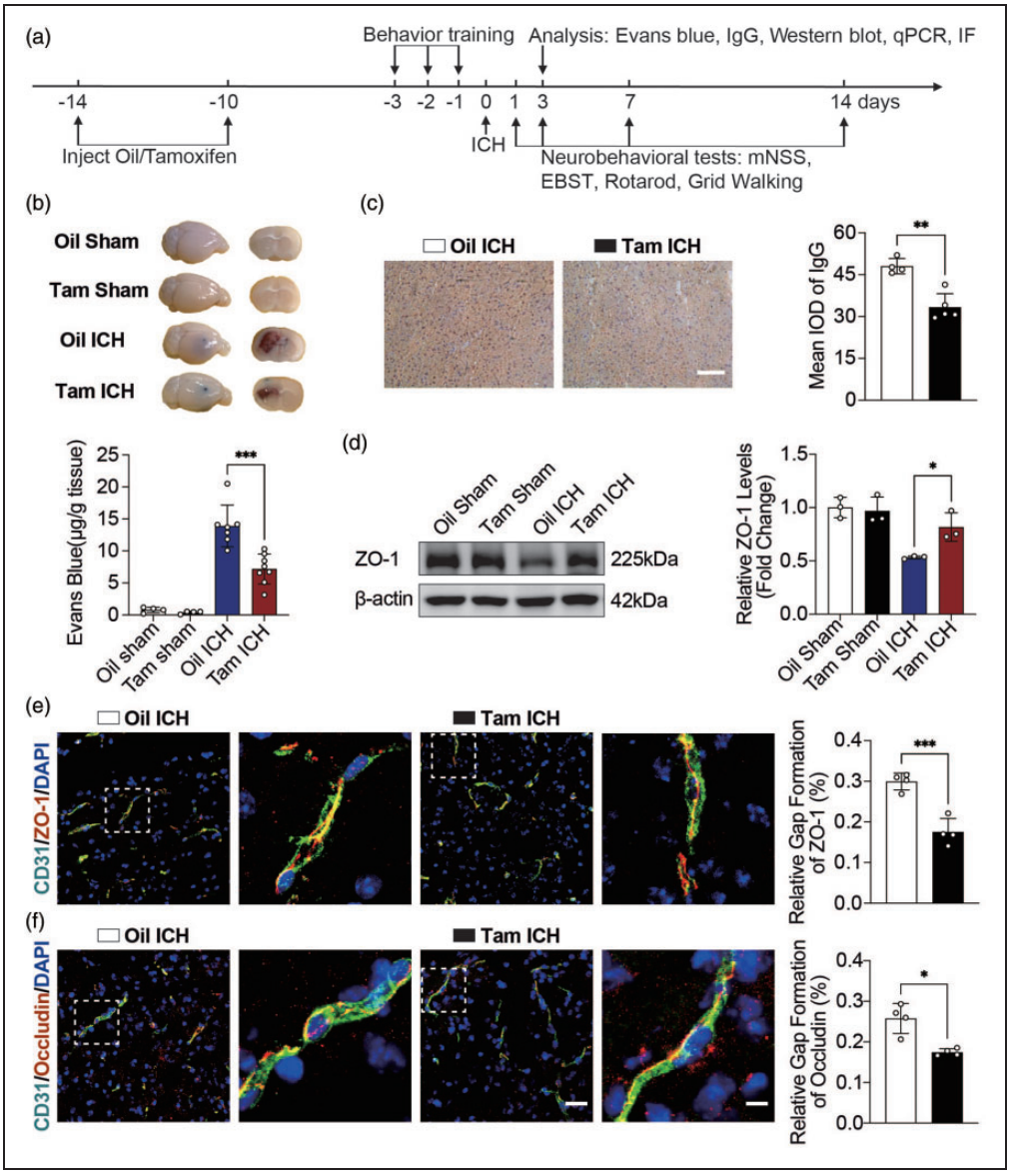


**Figure 3.** Knockout CCL5 in astrocytes attenuated BBB damage. (a) Schematic diagram of the experimental design. mNSS, modified neurologic severity score; EBST, elevated body swing test; IF, immunofluorescent staining; IgG, immunoglobulin G. (b) Representative perfused whole brains and 2 mm brain sections after EB injection in Oil Sham, Tam Sham, Oil ICH and Tam ICH groups. Quantification of extravasated EB from brains after EB injection in Oil Sham, Tam Sham, Oil ICH and Tam ICH groups. n = 4 mice in Oil Sham and Tam Sham groups (1 female, 3 male), n = 7 mice in Oil ICH group (2 female, 5 male), n = 8 mice in Tam ICH group (2 female, 6 male). One-way ANOVA with Tukey's multiple comparisons test. (c) Representative immunostaining images of IgG leakage in the hemorrhagic perifocal area at day 3 of ICH in Oil ICH and Tam ICH groups. Scale bar = 100 μm. Semi-quantification of IgG intensity in the hemorrhagic perifocal area at day 3 of ICH in Oil ICH and Tam ICH groups. n = 4 mice in Oil ICH group (2 female, 2 male), n = 5 mice in Tam ICH group (2 female, 3 male). Two-sided, unpaired Student's test. (d) Representative immunoblots of ZO-1 protein expression levels in the hemorrhagic perifocal area at day 3 of ICH in Oil Sham, Tam Sham, Oil ICH and Tam ICH groups. Quantification of ZO-1 protein expression levels in the hemorrhagic perifocal area at day 3 of ICH in Oil Sham, Tam Sham, Oil ICH and Tam ICH groups. n = 3 mice per group (2 female, 1 male). β-actin was used as an internal control. One-way ANOVA with Tukey's multiple comparisons test. (e) Representative immunostaining images of CD31 (green) and ZO-1 (red) in the hemorrhagic perifocal area at day 3 of ICH in Oil ICH and Tam ICH groups. Semi-quantification of gap length of ZO-1 in the hemorrhagic perifocal area at day 3 of ICH in Oil ICH and Tam ICH groups. n = 4 mice per group (2 female, 2 male). Two-sided, unpaired Student's test and (f) Representative immunostaining images of CD31 (green) and Occludin (red) in the hemorrhagic perifocal area at day 3 of ICH in Oil ICH and Tam ICH groups. Left scale bar = 50 μm, right scale bar = 10 μm. Semi-quantification of gap length of Occludin in the hemorrhagic perifocal area at day 3 of ICH in Oil ICH and Tam ICH groups. n = 4 mice per group (Oil ICH group all male, Tam ICH group 1 female, 3 male). Two-sided, Welch's t test. All data are presented as mean ± SD. *$p < 0.05$, **$p < 0.01$, ***$p < 0.001$.

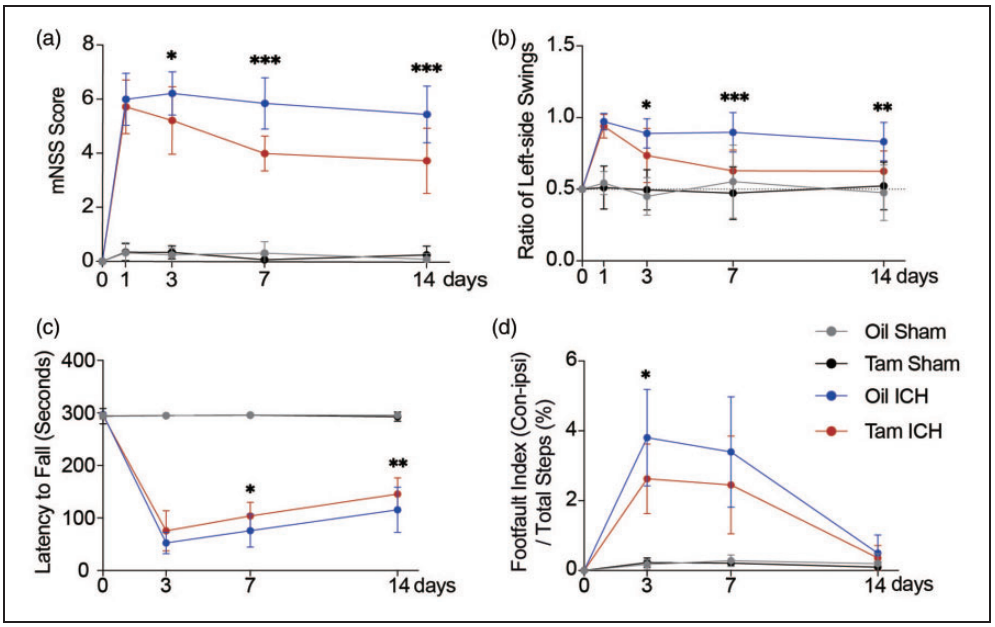


**Figure 4.** Knockout CCL5 in astrocytes improved neurobehavioral recovery in mice after ICH. (a–d) Neurobehavioral outcomes of Tam Sham, Oil Sham, Tam ICH and Oil ICH groups were assessed by four neurobehavioral tests including mNSS (a), EBST (b), rotarod test (c), and grid walking test (d). mNSS (a), EBST (b), rotarod test (c), n = 14 mice in Oil Sham, Oil ICH and Tam ICH groups (7 female, 7 male), n = 13 mice in Tam Sham group (7 female, 6 male). Grid walking test (d), n = 12 mice in Oil Sham and Tam Sham groups (6 female, 6 male), n = 9 mice in Oil ICH and Tam ICH groups (3 female, 6 male). Two-way ANOVA with Bonferroni multiple comparisons test. All data are presented as mean ± SD. *$p < 0.05$, **$p < 0.01$, ***$p < 0.001$.

suggesting that specific knockout of astrocytic CCL5 had neuroprotective effects.

## *$CD8^+$ T cells aggravated brain injury by inducing apoptosis of ECs in hemorrhagic stroke mice*

Our above findings suggested that astrocytic CCL5 mediated the infiltration of $CD8^+$ T cells into hemorrhagic brain, and inhibition of this process attenuated BBB disruption, leading us to hypothesize that $CD8^+$ T cells may modulate BBB integrity after hemorrhagic stroke. TUNEL staining results showed that apoptosis of ECs was reduced in astrocytic CCL5 knockout mice compared with the control group (Figure 5(a)). Interestingly, transplantation of $CD8^+$ T cells into Tam ICH mice but not Tam Sham mice increased apoptosis of ECs (Figure 5(b) and (c)), EB leakage (Figure 5(d)) and IgG leakage (Figure 5(e) and (f)), suggesting that $CD8^+$ T cells disrupted BBB by inducing apoptosis of ECs.

## *$CD8^+$ T cells induce apoptosis of ECs via perforin and granzyme B*

It is well documented that $CD8^+$ T cells induce cell death through perforin and granzyme.[30] Western blot showed that perforin and granzyme B were increased in hemorrhagic stroke mice, and decreased in astrocytic CCL5 knockout mice compared with the control group (Figure 6(a) to (c)).

$Ca^{2+}$ chelator EGTA, a perforin inhibitor, can inhibit perforin to protect cells viability.[31] bEnd.3 cells were treated with 0, 0.05, 0.1, 0.2, 0.4, 0.5, 1, and 2 mM EGTA for 24 h, respectively, and the viability of bEnd.3 cells was tested by CCK-8. CCK-8 results showed that the viability of bEnd.3 cells was still up to 94.7% when the EGTA concentration was 0.2 mM. However, when the EGTA concentration was higher than 0.2 mM, the viability of bEnd.3 cells was significantly reduced (Suppl. Fig. 9A). Therefore, we chose 0.2 mM EGTA for further study.

To investigate the effects of $CD8^+$ T cells on the viability of bEnd.3 cells *in vitro*, $CD8^+$ T cells isolated from hemorrhagic stroke mice were co-cultured with bEnd.3 cells using transwell. bEnd.3 cells and $CD8^+$ T cells were co-cultured at cell ratios of 1:2, 1:5, 1:10 and 1:20 for 24 h and 48 h, respectively. CCK-8 results showed that both $CD8^+$ T and bEnd.3 cells were in the best condition when the cell ratio was 1:5 and co-cultured for 24 h (Suppl. Fig. 9B). Therefore, 1:5 cell ratio and 24 h co-culture were selected as the optimal cell ratio and time. $CD8^+$ T cells and bEnd.3 cells were subsequently co-cultured for 24 h in the presence or absence of EGTA. CCK-8 results showed

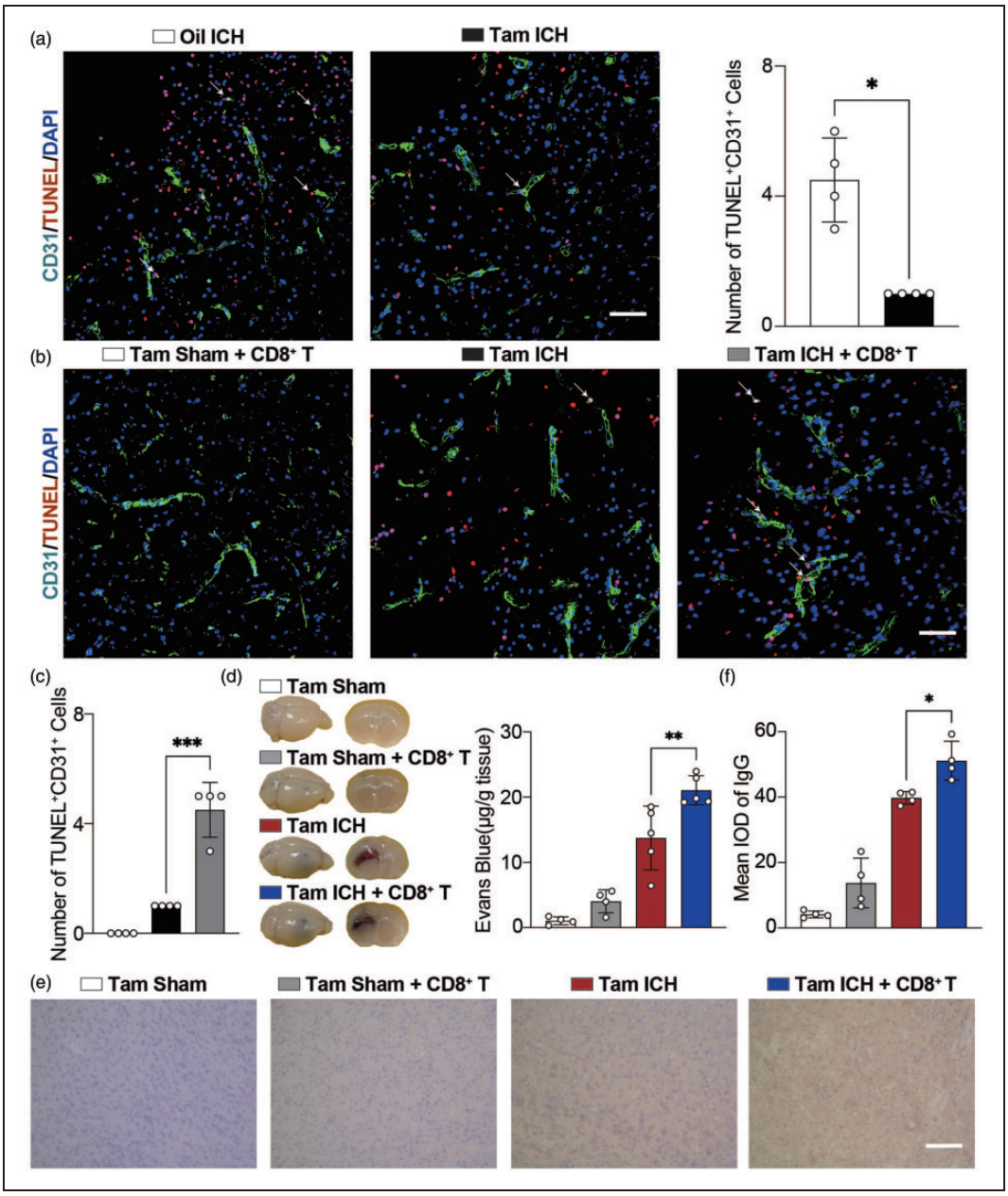


**Figure 5.** $CD8^+$ T cells transplantation aggravated apoptosis of ECs. (a) Representative immunostaining images of CD31 (green) with TUNEL (red) in the hemorrhagic perifocal area at day 3 of ICH in Oil ICH and Tam ICH groups. Scale bar = 50 μm. Arrowheads indicate the colocalization of CD31 with TUNEL. Number of apoptotic ECs in the hemorrhagic perifocal area at day 3 of ICH in Oil ICH and Tam ICH groups. n = 4 mice per group (all male). Two-sided, Welch's t test. (b) Representative immunostaining images of CD31 (green) with TUNEL (red) in the hemorrhagic perifocal area at day 3 of ICH in Tam Sham + $CD8^+$ T, Tam ICH, and Tam ICH + $CD8^+$ T groups. Scale bar = 50 μm. Arrowheads indicate the colocalization of CD31 with TUNEL. (c) Number of apoptotic ECs in the hemorrhagic perifocal area at day 3 of ICH in Tam Sham + $CD8^+$ T, Tam ICH, and Tam ICH + $CD8^+$ T groups. n = 4 mice per group (2 female, 2 male). One-way ANOVA with Tukey's multiple comparisons test. (d) Representative perfused whole brains and 2 mm brain sections after EB injection in Tam Sham, Tam Sham + $CD8^+$ T, Tam ICH and Tam ICH + $CD8^+$ T groups. Quantification of extravasated EB from brains after EB injection in Tam Sham, Tam Sham + $CD8^+$ T, Tam ICH, and Tam ICH + $CD8^+$ T groups. n = 4 mice in Tam Sham and Tam Sham + $CD8^+$ T groups (3 female, 1 male), n = 5 mice in Tam ICH group (3 female, 2 male), n =5 mice in Tam ICH + $CD8^+$ T group (2 female, 3 male). One-way ANOVA with Tukey's multiple comparisons test and (e) Representative immunostaining images of IgG leakage in the hemorrhagic perifocal area in Tam Sham, Tam Sham + $CD8^+$ T, Tam ICH, and Tam ICH + $CD8^+$ T groups. Scale bar = 100 μm. F. Semi-quantification of IgG intensity in the hemorrhagic perifocal area in Tam Sham, Tam Sham + $CD8^+$ T, Tam ICH, and Tam ICH + $CD8^+$ T groups. n = 4 mice per group (2 female, 2 male). One-way ANOVA with Tukey's multiple comparisons test. All data are presented as mean ± SD. *$p < 0.05$, **$p < 0.01$, ***$p < 0.001$.

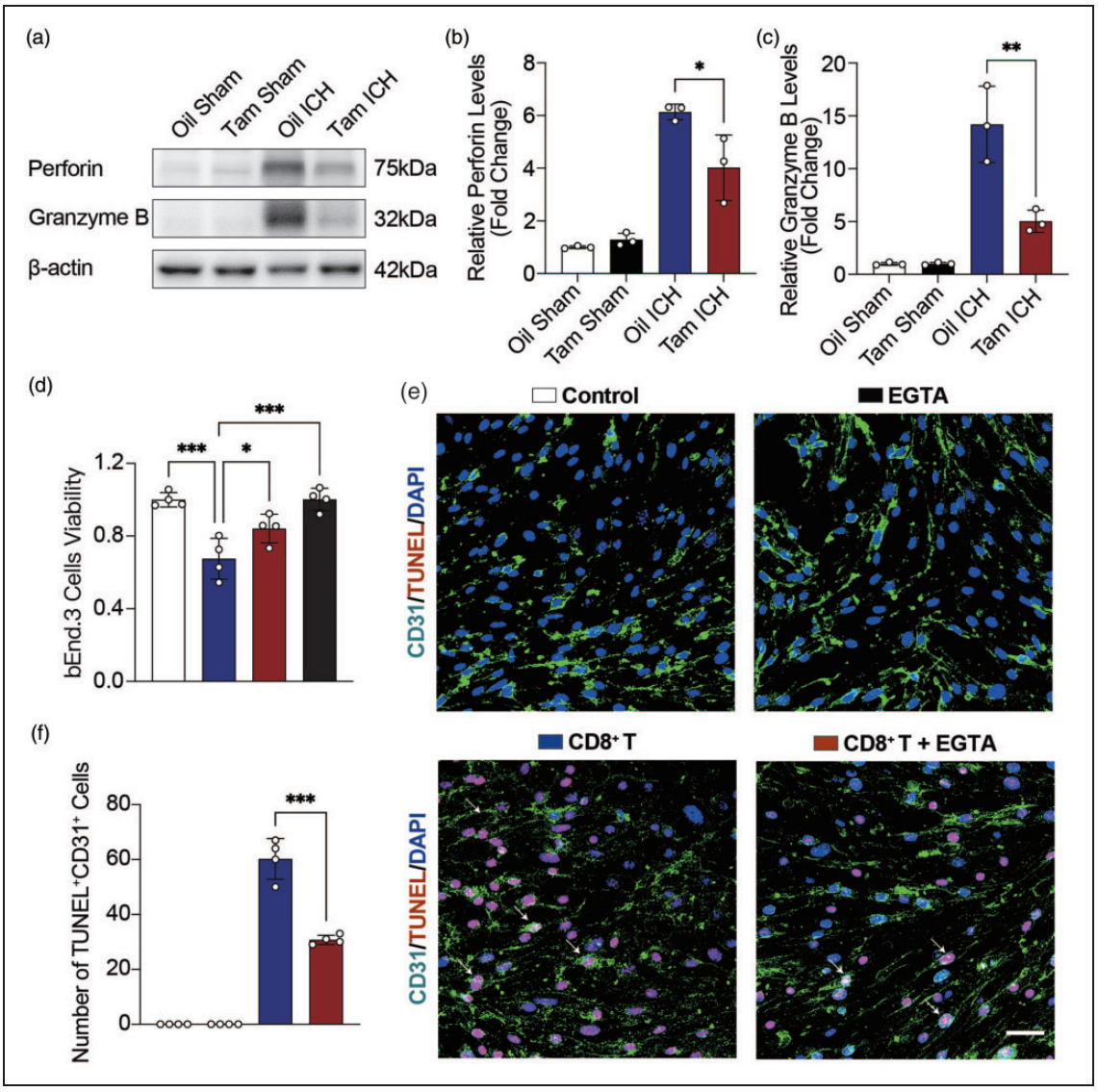


**Figure 6.** Inhibition of perforin reduced apoptosis of ECs. (a) Representative immunoblots of Perforin and Granzyme B protein expression levels in the hemorrhagic perifocal area in Oil Sham, Tam Sham, Oil ICH and Tam ICH groups. (b, c) Quantification of Perforin (b) and Granzyme B (c) protein expression levels in the hemorrhagic perifocal area in Oil Sham, Tam Sham, Oil ICH and Tam ICH groups. n = 3 mice per group (2 female, 1 male). β-actin was used as an internal control. One-way ANOVA with Tukey's multiple comparisons test. (d) Statistics of bEnd.3 cells viability by CCK8 in Control, $CD8^+$ T, $CD8^+$ T + EGTA, and EGTA groups. n = 4 biologically independent bEnd.3 cell cultures. One-way ANOVA with Tukey's multiple comparisons test. (e) Representative immunostaining images of CD31 (green) with TUNEL (red) in Control, $CD8^+$ T, $CD8^+$ T + EGTA, and EGTA groups. Scale bar = 50 μm. Arrowheads indicate the colocalization of CD31 with TUNEL and (f) Number of apoptotic bEnd.3 cells in Control, $CD8^+$ T, $CD8^+$ T + EGTA, and EGTA groups. n = 4 biologically independent bEnd.3 cell cultures. One-way ANOVA with Tukey's multiple comparisons test. All data are presented as mean ± SD. *$p < 0.05$, **$p < 0.01$, ***$p < 0.001$.

that $CD8^+$ T cells decreased the viability of bEnd.3 cells, while EGTA inhibited the effect of perforin and promoted the viability of bEnd.3 cells (Figure 6 (d)). TUNEL staining also showed that $CD8^+$ T cells induced apoptosis of bEnd.3 cells, while EGTA inhibited the effect of perforin, which reduced the apoptosis of bEnd.3 cells (Figure 6(e) and (f)).

## Discussion

Reactive astrocytes act as a double-edged sword on the injured brain.[32,33] As an important component of BBB, astrocytes regulate BBB integrity through both direct and indirect mechanisms, including secreting multiple factors or cross-talk with immune cells to regulate the

function of ECs.[34] Our current research demonstrated that astrocytic CCL5 mediated the infiltration of $CD8^+$ T cells into the brain after hemorrhagic stroke, and infiltrated $CD8^+$ T cells induced apoptosis of ECs via perforin and granzyme B. Our study indicated a novel mechanism that mediated astrocyte-T cell interaction and elucidated how this interaction affected the outcomes of hemorrhagic stroke.

The heterogeneity of astrocytes is well-recognized and has been reported in several CNS injuries including stroke.[35,36] Liddelow et al. reported that microglia-derived IL-1α, TNF and C1q induced phenotypic change of astrocytes into neurotoxic astrocytes (A1 astrocytes).[37] Our previous studies demonstrated the presence of neurotoxic astrocytes in the brain after ischemic stroke, and inhibiting phenotypic change of neurotoxic astrocytes reduced BBB disruption,[17] but its mechanism was still unclear. Through RNA sequencing, we found that a series of chemokines, including CCL7, CCL5, CXCL5, CXCL1 and CCL2, were highly expressed in reactive astrocytes, of which CCL5 is one of the most up-regulated genes. We also verified CCL5 expression in the brain of mice with hemorrhagic stroke, and proved that CCL5 was highly up-regulated in reactive astrocytes.

CCL5 is a small molecular protein consisting of 68 amino acids, which can bind to specific receptors in the seven-transmembrane G protein-coupled receptor (GCPR) family, including CCR1, CCR3, CCR4 and CCR5.[27,38] The increase of CCL5 is related to various inflammatory diseases and pathological conditions, such as central nervous system diseases and cancer, which act as chemokines by promoting the infiltration of immune cells.[29,38] However, the role of CCL5 in different diseases remains controversial. CCL5 has been demonstrated to mediate pro-inflammatory response in chronic systemic infection mice.[39] In contrast, Tokami et al. have shown that CCL5 up-regulated neurotrophic factors and neuron survival via Akt and Erk1/2 pathway.[40] In the present study, we found that expression of CCL5 specifically increased in reactive astrocytes of hemorrhagic brain, and knockout astrocytic CCL5 attenuated BBB disruption, as well as improved neurobehavioral outcomes in stroke mice, which indicated that CCL5 derived from reactive astrocytes was involved in destroying BBB integrity, at least in the hemorrhagic stroke brain.

As an important chemokine, CCL5 has been proven to play an important role in recruiting immune cells.[27,28] In ischemic stroke, hemocyte-derived CCL5 recruited white blood cells and platelets into the cerebral microvascular system after stroke, resulting in increased BBB permeability and tissue infarction.[41] Our research demonstrated that CCL5 promoted the infiltration of $CD8^+$ T cells into the hemorrhagic mouse brain, but not other immune cells, which could be related to the detection time. For example, neutrophil accumulation in the ischemic hemisphere increased after 3 h of stroke, reaching a maximum after 24 h,[42] while in our study we examined immune cell infiltration at 3 days after stroke. In addition, Huffman et al. found that CCL5 derived from myeloid cells mediated an influx of $CD4^+$ T cells but not $CD8^+$ T cells into the tumor microenvironment,[43] suggesting CCL5 secreted from different cells may play distinct roles in different pathologies.

Previous studies indicated that both $CD4^+$ T cells and $CD8^+$ T cells exert detrimental effects on early stroke.[44] Depletion of $CD4^+$ T cells or $CD8^+$ T cells reduced infarct volume after the transient middle cerebral artery occlusion (tMCAO).[45] In our study, specific knockout of CCL5 in astrocytes reduced $CD8^+$ T cells infiltration to the brain as well as attenuated BBB disruption, and injection of $CD8^+$ T cells reversed such protective effect, suggesting $CD8^+$ T cells played a detrimental role in hemorrhagic stroke via disrupting BBB integrity. It is well known that $CD8^+$ T cells are the main source of perforin and granzyme.[46,47] Liu and colleagues revealed that perforin derived from $CD8^+$ T cells destroyed the blood-spinal cord barrier (BSCB) after spinal cord injury (SCI), increased its permeability, and led to inflammatory factor infiltration and aggravated secondary injury.[48] Huggins et al. reported that perforin secreted by $CD8^+$ T cells caused fatal brain edema during experimental cerebral malaria.[49] Granzyme B, a member of the serine protease family, acts synergistically with perforin to induce cell apoptosis.[50] Our study showed that perforin and granzyme B were up-regulated at 3 days after hemorrhagic stroke, and blocking perforin reduced apoptosis of ECs. However, it should be noted that perforin-granzyme pathway may not be the only way that mediates $CD8^+$ T cells induced cell death,[51] whether other signals are involved in this process needs to be further studied.

One limitation of this study is that we did not compare the differences between male and female $Aldh1l1^{CreERT2+/-}$: $CCL5^{f/f}$ mice in each experimental assessment endpoint. However, sexual dimorphism has been reported in many aspects, including cerebral blood flow regulation, response to stroke etc. A recent study showed that males and females have different middle cerebral blood velocities during both poikilocapnia and hypercapnia, suggesting sex can influence cerebral hemodynamics.[52] A review written by Cheryl D Bushnell et al. indicates that biologic sex affects many variables that are important to stroke,

such as general health status, cerebrovascular anatomy and function, unique risk factors (such as pregnancy and preeclampsia), symptomatology, and therapeutic response.[53] Sex also has impact on the therapeutic efficacy of drugs for stroke. For example, inhibition of focal adhesion kinase (FAK) reduced brain injury size, neuroinflammation and motor dysfunction in female stroke mice but not in male stroke mice.[54] Whether there are gender differences in the performance of astrocytes-specific CCL5 knockout mice after ICH is worth investigating and being incorporated into future studies.

Overall, our current study revealed the critical role of reactive astrocytes in immune response, neuroinflammation, and BBB dysfunction after stroke. In addition, astrocytes may affect many other pathophysiological processes after brain injury. Amy R Nippert et al. found that astrocytes contribute to hypoglycemia-induced increases in cerebral blood flow by releasing vasodilators in a $Ca^{2+}$-dependent manner.[55] A review written by our lab highlights that astrocytes participate in myelin elimination in the developing brain, and during CNS diseases, astrocytes are also involved in clearing degenerated myelin debris to accelerate remyelination.[56] Shibahara reported that pericyte-conditioned medium-treated astrocytes increased the expression of laminin α2, and promoted remodeling of key extracellular matrix proteins after stroke, which leads to oligodendrogenesis.[57] In conclusion, our study provides important new insights into the mechanism of immune-mediated BBB damage in ICH. After ICH, astrocytes are activated and secrete CCL5 to recruit $CD8^+$ T cell infiltration into the brain, subsequentially kill ECs by releasing perforin and granzyme B, exacerbating the damage of BBB. Our data provides a new idea for the treatment of stroke.

## Funding

The author(s) disclosed receipt of the following financial support for the research, authorship, and/or publication of this article: This study was supported by grants from Shanghai Rising Star (21QA1405200 [YT]), the National Natural Science Foundation of China (82071284 [YT], 82371307 [YT], 82172529 [JW], 81974179 [ZZ], 82271320 [ZZ], 32301146 [WL]), National Key R&D Program of China (2019YFA0112000 [YT], 2022YFA1603600 [ZZ]), Young Leading Scientists Cultivation Plan supported by Shanghai Municipal Education Commission (ZXWH1082101, [YT]), the Fundamental Research Funds for the Central Universities (YG2023ZD02, [YT]), Shanghai Sailing Program (23YF1420700 [WL]), Scientific Research and Innovation Program of Shanghai Education Commission (2019-01-07-00-02-E00064 [GYY]), Scientific and Technological Innovation Act Program of Shanghai Science and Technology Commission (20JC1411900 [GYY]), and SUITM-202306 [YT].

## Acknowledgements

We would like to thank Dr. Won-Suk Chung for the gift of $Aldh1l1^{CreERT2+/-}$ mice and Dr. Qidong Zu and his OE Biotech Company (Shanghai, China, http://www.oebiotech.com/) for assistance with the bioinformatics analysis of RNA-seq.

## Declaration of conflicting interests

The author(s) declared no potential conflicts of interest with respect to the research, authorship, and/or publication of this article.

## Authors' contributions

All the authors agree to the publication of this work. YT, GYY, ZZ, and WL designed the experiments and helped to edit the manuscript finally. SZ, CL, and JW performed the experiments, analyzed the data, and wrote the manuscript. JY contributed to the flow cytometry experiments. QL, LG, and SD contributed to animal identification and neurobehavioral testing. TX and YG are helpful for EB detection. All the authors edited and reviewed the manuscript.

## Supplementary material

Supplemental material for this article is available online.

## ORCID iD

Yaohui Tang https://orcid.org/0000-0002-9603-2650

## References

1. Daneman R and Prat A. The blood-brain barrier. *Cold Spring Harb Perspect Biol* 2015; 7: a020412.
2. Huang X, Hussain B and Chang J. Peripheral inflammation and blood-brain barrier disruption: effects and mechanisms. *CNS Neurosci Ther* 2021; 27: 36–47.
3. Pivoriūnas A and Verkhratsky A. Astrocyte–endotheliocyte axis in the regulation of the blood–brain barrier. *Neurochem Res* 2021; 46: 2538–2550.
4. Tschoe C, Bushnell CD, Duncan PW, et al. Neuroinflammation after intracerebral hemorrhage and potential therapeutic targets. *J Stroke* 2020; 22: 29–46.
5. Sukumari-Ramesh S, Alleyne CH and Dhandapani KM. Astrogliosis: a target for intervention in intracerebral hemorrhage? *Transl Stroke Res* 2012; 3: 80–87.
6. Lively S and Schlichter LC. Age-related comparisons of evolution of the inflammatory response after intracerebral hemorrhage in rats. *Transl Stroke Res* 2012; 3: 132–146.
7. Chiu CD, Yao NW, Guo JH, et al. Inhibition of astrocytic activity alleviates sequela in acute stages of intracerebral hemorrhage. *Oncotarget* 2017; 8: 94850–94861.
8. Han RT, Kim RD, Molofsky AV, et al. Astrocyte-immune cell interactions in physiology and pathology. *Immunity* 2021; 54: 211–224.
9. Shi SX, Vodovoz SJ, Xiu Y, et al. T-lymphocyte interactions with the neurovascular unit: implications in intracerebral hemorrhage. *Cells* 2022; 11: 2011.

10. Aronowski J and Zhao X. Molecular pathophysiology of cerebral hemorrhage secondary brain injury. *Stroke* 2011; 42: 1781–1786.
11. Sangha N and Gonzales NR. Treatment targets in intracerebral hemorrhage. *Neurotherapeutics* 2011; 8: 374–387.
12. Madangarli N, Bonsack F, Dasari R, et al. Intracerebral hemorrhage: blood components and neurotoxicity. *Brain Sci* 2019; 9: 316.
13. Li M, Ren H, Sheth KN, et al. A TSPO ligand attenuates brain injury after intracerebral hemorrhage. *FASEB J* 2017; 31: 3278–3287.
14. Durrant DM, Williams JL, Daniels BP, et al. Chemokines referee inflammation within the central nervous system during infection and disease. *Adv Med* 2014; 2014: 806741.
15. Kunkl M, Amormino C, Tedeschi V, et al. Astrocytes and inflammatory T helper cells: a dangerous liaison in multiple sclerosis. *Front Immunol* 2022; 13: 824411. Review.
16. Kim RY, Hoffman AS, Itoh N, et al. Astrocyte CCL2 sustains immune cell infiltration in chronic experimental autoimmune encephalomyelitis. *J Neuroimmunol* 2014; 274: 53–61.
17. Zhang Q, Liu C, Shi R, et al. Blocking C3d +/GFAP + A1 astrocyte conversion with semaglutide attenuates blood-brain barrier disruption in mice after ischemic stroke. *Aging Dis* 2022; 13: 943–959.
18. Qian B, Zhaofu S, Yang L, et al. Intracerebral haemorrhage: from clinical settings to animal models. *Stroke and Vascular Neurology* 2020; 5: 388.
19. Lei B, Sheng H, Wang H, et al. Intrastriatal injection of autologous blood or clostridial collagenase as murine models of intracerebral hemorrhage. *J Vis Exp* 2014; 89: 51439.
20. Yang Y, Ren J, Sun Y, et al. A connexin43/Yap axis regulates astroglial-mesenchymal transition in hemoglobin induced astrocyte activation. *Cell Death Differ* 2018; 25: 1870–1884.
21. Tang G, Liu Y, Zhang Z, et al. Mesenchymal stem cells maintain blood-brain barrier integrity by inhibiting aquaporin-4 upregulation after cerebral ischemia. *Stem Cells* 2014; 32: 3150–3162.
22. Shi X, Luo L, Wang J, et al. Stroke subtype-dependent synapse elimination by reactive gliosis in mice. *Nat Commun* 2021; 12: 6943–6943.
23. Muyassar M, Lu J, Yaying S, et al. Plasma from healthy donors protects blood–brain barrier integrity via FGF21 and improves the recovery in a mouse model of cerebral ischaemia. *Stroke Vasc Neurol* 2021; 6: 561.
24. Chen T, Shi R, Suo Q, et al. Progranulin released from microglial lysosomes reduces neuronal ferroptosis after cerebral ischemia in mice. *J Cereb Blood Flow Metab* 2023; 43: 505–517.
25. Xie W, Huang T, Guo Y, et al. Neutrophil-derived cathelicidin promotes cerebral angiogenesis after ischemic stroke. *J Cereb Blood Flow Metab* 2023; 43: 1503–1518.
26. Kim MO, Suh HS, Brosnan CF, et al. Regulation of RANTES/CCL5 expression in human astrocytes by interleukin-1 and interferon-$\beta$. *J Neurochem* 2004; 90: 297–308.
27. Barnes DA, Huston M, Holmes R, et al. Induction of RANTES expression by astrocytes and astrocytoma cell lines. *J Neuroimmunol* 1996; 71: 207–214.
28. Schall TJ, Bacon K, Toy KJ, et al. Selective attraction of monocytes and T lymphocytes of the memory phenotype by cytokine RANTES. *Nature* 1990; 347: 669–671.
29. Meurer R, Van Riper G, Feeney W, et al. Formation of eosinophilic and monocytic intradermal inflammatory sites in the dog by injection of human RANTES but not human monocyte chemoattractant protein 1, human macrophage inflammatory protein 1 alpha, or human interleukin 8. *J Exp Med* 1993; 178: 1913–1921.
30. Mracsko E, Liesz A, Stojanovic A, et al. Antigen dependently activated cluster of differentiation 8-positive T cells cause perforin-mediated neurotoxicity in experimental stroke. *J Neurosci* 2014; 34: 16784–16795.
31. Zhou Z, He H, Wang K, et al. Granzyme a from cytotoxic lymphocytes cleaves GSDMB to trigger pyroptosis in target cells. *Science* 2020; 368: eaaz7548.
32. Morizawa YM, Hirayama Y, Ohno N, et al. Reactive astrocytes function as phagocytes after brain ischemia via ABCA1-mediated pathway. *Nat Commun* 2017; 8: 28.
33. Kim H, Leng K, Park J, et al. Reactive astrocytes transduce inflammation in a blood-brain barrier model through a TNF-STAT3 signaling axis and secretion of alpha 1-antichymotrypsin. *Nat Commun* 2022; 13: 6581.
34. Michinaga S and Koyama Y. Dual roles of astrocyte-derived factors in regulation of blood-brain barrier function after brain damage. *Int J Mol Sci* 2019; 20: 571.
35. Moulson AJ, Squair JW, Franklin RJM, et al. Diversity of reactive astrogliosis in CNS pathology: heterogeneity or plasticity? *Front Cell Neurosci* 2021; 15: 703810. Review.
36. Qiu M, Zong JB, He QW, et al. Cell heterogeneity uncovered by single-cell RNA sequencing offers potential therapeutic targets for ischemic stroke. *Aging Dis* 2022; 13: 1436–1454.
37. Liddelow SA, Guttenplan KA, Clarke LE, et al. Neurotoxic reactive astrocytes are induced by activated microglia. *Nature* 2017; 541: 481–487.
38. Appay V and Rowland-Jones SL. RANTES: a versatile and controversial chemokine. *Trends Immunol* 2001; 22: 83–87.
39. Ádám D, Neil H, Thomas EL, et al. Chronic systemic infection exacerbates ischemic brain damage via a CCL5 (regulated on activation, normal T-Cell expressed and secreted)-mediated proinflammatory response in mice. *J Neurosci* 2010; 30: 10086.
40. Tokami H, Ago T, Sugimori H, et al. RANTES has a potential to play a neuroprotective role in an autocrine/paracrine manner after ischemic stroke. *Brain Res* 2013; 1517: 122–132.
41. Terao S, Yilmaz G, Stokes KY, et al. Blood cell-derived RANTES mediates cerebral microvascular dysfunction, inflammation, and tissue injury after focal ischemia-reperfusion. *Stroke* 2008; 39: 2560–2570.

42. Gelderblom M, Leypoldt F, Steinbach K, et al. Temporal and spatial dynamics of cerebral immune cell accumulation in stroke. *Stroke* 2009; 40: 1849–1857.
43. Huffman AP, Lin JH, Kim SI, et al. CCL5 mediates CD40-driven CD4+ T cell tumor infiltration and immunity. *JCI Insight* 2020; 5: e137263.
44. Lei T-Y, Ye Y-Z, Zhu X-Q, et al. The immune response of T cells and therapeutic targets related to regulating the levels of T helper cells after ischaemic stroke. *J Neuroinflammation* 2021; 18: 25.
45. Liesz A, Zhou W, Mracskó É, et al. Inhibition of lymphocyte trafficking shields the brain against deleterious neuroinflammation after stroke. *Brain* 2011; 134: 704–720.
46. Liu Y, Zhang T, Zhou Y, et al. Visualization of perforin/gasdermin/complement-formed pores in real cell membranes using atomic force microscopy. *Cell Mol Immunol* 2019; 16: 611–620.
47. Yao Y, Chen S, Cao M, et al. Antigen-specific CD8+ T cell feedback activates NLRP3 inflammasome in antigen-presenting cells through perforin. *Nat Commun* 2017; 8: 15402.
48. Liu Z, Zhang H, Xia H, et al. CD8 T cell-derived perforin aggravates secondary spinal cord injury through destroying the blood-spinal cord barrier. *Biochem Biophys Res Commun* 2019; 512: 367–372.
49. Huggins MA, Johnson HL, Jin F, et al. Perforin expression by CD8 T cells is sufficient to cause fatal brain edema during experimental cerebral malaria. *Infect Immun* 2017; 85: e00985–00916.
50. Pinkoski MJ, Hobman M, Heibein JA, et al. Entry and trafficking of granzyme B in target cells during granzyme B-perforin-mediated apoptosis. *Blood* 1998; 92: 1044–1054.
51. Schäfer S and Zernecke A. CD8+ T cells in atherosclerosis. *Cells* 2020; 10: 37.
52. Panerai RB, Davies A, Clough RH, et al. The effect of hypercapnia on the directional sensitivity of dynamic cerebral autoregulation and the influence of age and sex. *J Cereb Blood Flow Metab* 2023; 5: 271678X2 31203475.
53. Bushnell CD, Chaturvedi S, Gage KR, et al. Sex differences in stroke: challenges and opportunities. *J Cereb Blood Flow Metab* 2018; 38: 2179–2191.
54. Jia C, Lovins C, Malone HM, et al. Female-specific neuroprotection after ischemic stroke by vitronectin-focal adhesion kinase inhibition. *J Cereb Blood Flow Metab* 2022; 42: 1961–1974.
55. Nippert AR, Chiang PP, Del Franco AP, et al. Astrocyte regulation of cerebral blood flow during hypoglycemia. *J Cereb Blood Flow Metab* 2022; 42: 1534–1546.
56. Xu T, Liu C, Deng S, et al. The roles of microglia and astrocytes in myelin phagocytosis in the central nervous system. *J Cereb Blood Flow Metab* 2023; 43: 325–340.
57. Shibahara T, Nakamura K, Wakisaka Y, et al. PDGFRbeta-positive cell-mediated post-stroke remodeling of fibronectin and laminin alpha2 for tissue repair and functional recovery. *J Cereb Blood Flow Metab* 2023; 43: 518–530.